Proceedings of the Canadian Society for Mechanical Engineering International Congress
32nd Annual Conference of the Computational Fluid Dynamics Society of Canada
Canadian Society of Rheology Symposium
CSME-CFDSC-CSR 2025
May 25–28, 2025, Montréal, Québec, Canada

Effect of Rotor Solidity on the Aeroacoustics Behaviour of Automotive Cooling Fan Module

Tayyab Akhtar[1], Stephane Moreau[1], Bruno Demory[2], Manuel Henner[2]
[1]Department of Mechanical Engineering,Université de Sherbrooke,
2500 Boulevard de l'Université, Sherbrooke, QC J1K 2R1, Canada

[2] Simulation and Reliability Discipline, Valeo Power,
78320 La Verrière, France

Abstract— This study analyzes the flow and acoustic characteristics of a low-speed axial flow fan with a rotating ring, focusing on the influence of rotor solidity on noise emission and its directivity. Two rotor configurations, one with seven blades and the other with thirteen, are evaluated at identical flow rates. Numerical simulations are performed using the Lattice-Boltzmann Method (LBM) on an automotive cooling module comprising a shroud, fan, and heat exchanger, employing a medium grid resolution. The findings indicate that increased rotor solidity leads to greater leakage flow and higher thrust fluctuations. However, higher solidity promotes a more uniform flow on the blade surface, reducing negative pressures near the leading edge on the suction side. Simultaneous far-field noise predictions are conducted using an arc of microphones, and the results are compared with experimental data for the seven-bladed rotor. Despite a significant reduction in rotational speed, the thirteen-bladed rotor exhibits more pronounced sub-harmonic humps, characterized by strong vortical structures from leakage flow, compared to the seven-bladed rotor. Sound pressure level spectra calculated at two different operating points show good agreement with experimental data in the high-frequency broadband range, while the thirteen-bladed rotor demonstrates higher amplitudes at lower frequencies where tip leakage noise mostly affects. Sound directivity comparisons for both operating points reveal a consistent dipole radiation pattern, with higher amplitudes along the rotational axis and lower values in the rotational plane for both rotors but higher amplitudes for increased solidity.

Keywords- Automotive-Fan; Rotor-solidity; Aeroacoustics; Axial fan noise,

I. INTRODUCTION

The thermal management system of an automobile heavily relies on the cooling module, typically located at the front of the vehicle. This module consists of at least one heat exchanger (HE) and a fan assembly, both designed to maximise heat transfer [1]. A critical component of this system is the low-speed axial fan, which plays a key role in determining the performance, stability, and lifespan of the engine and batteries. It is designed to drive airflow through the fins and louvers of the HE core at higher flow rates. The aerodynamic efficiency and noise produced by these fans significantly affect vehicle operation. In particular, the acoustic characteristics of these fans have become an increasingly important quality criterion, driven by rising comfort expectations and stricter noise regulations. Various design parameters, such as blade thickness, chord length, hub and tip shapes, blade stacking, aspect ratio, and hub-to-tip ratio influence the sound field generated by these fans. Even though numerous studies have already been published investigating these design factors. [1-6], there is limited research elaborating on the effect of blade count on axial flow fans [7]. According to existing literature, increasing the blade count at a constant speed leads to higher sound power generation [7]. However, in industrial applications, blade count is often increased to reduce rotational speed while maintaining the same flow rate as the sound power generated by such machines is proportional to the sixth power of speed. Notably, there is no comprehensive study on automotive fans that explores the impact of rotor solidity on radiated noise levels and directivity.

This gap motivates the present study, to reduce the rotational speed by increasing the rotor solidity. This objective is met while maintaining the same mass flow rate and axial packaging conditions. To investigate the effects of rotor solidity on the flow and sound fields, the commercial software PowerFLOW is utilized, which has already demonstrated its reliability in accurately predicting the aeroacoustic performance of axial cooling fans [8-11]. The configurations examined in this study are described in the next section, followed by a detailed explanation of the experimental setup. Subsequently, the numerical methodology is outlined, along with an analysis of the resulting velocity and pressure fields. The final section focuses on the aeroacoustic characteristics of the system and concludes with a summary of the key findings and their implications.

II. TESTED FAN CONFIGURATIONS

The studied cooling module is designed and supplied by Valeo Thermal Systems. This module comprises several key components: a fan, shroud, motor, heat exchanger, as illustrated in Fig. 1. The 7-bladed fan is taken as reference geometry and the 13-bladed fan is designed to achieve the same flow rate at the high-speed operating condition as the 7-bladed fan, but with a significantly reduced rotational speed. This design is achieved through a multi-objective optimization process using the I-Sight module from 3DS, which employed a design of experiments (DOE) approach. The DOE used an Optimal Latin Hypercube (OLH) sampling method for the distribution of different designs, and the NSGA-II algorithm was selected as the optimization method. Achieving such a reduction in rotational speed required a substantial increase in the number of blades and a complete redesign of the blade planform (chord and stagger angle distribution). For instance, the high forward sweep of the 7 blade fan could not be maintained in the optimization process, while maintaining blade efficiency and overall packaging. Both configurations are tested at two operating points, at free discharge and design point. In free discharge case the whole setup consists of all above mentioned components except heat exchanger whereas at design point complete package is installed. The 7-bladed rotor is simulated at constant rotational speed for both operating points whereas the rotational speed of 13-bladed rotor is adjusted to get the same mass flowrate as of 7-bladed fan as shown in Tab.1.

Table 1: Test configuration and operating conditions

Acronym	Parts	Speed	Mass Flow Rate
7B_noHE	Fan, Shroud, Motor	2500rpm	0.77kg/sec
7B_withHE	Fan, Shroud, Motor, HE	2500rpm	0.602kg/sec
13B_noHE	Fan, Shroud, Motor	2300rpm	0.77kg/sec
13B_withHE	Fan, Shroud, Motor, HE	2218rpm	0.602kg/sec

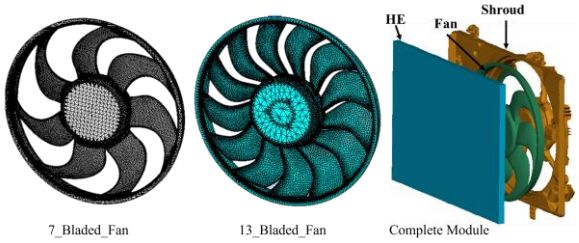

Figure 1: Rotors and complete module.

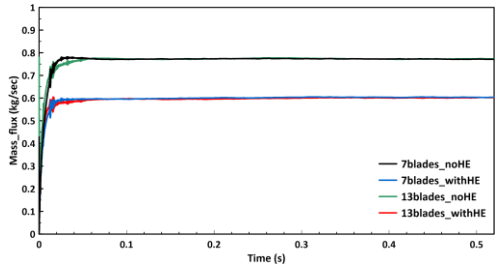

Figure 2: Operating point mass flow rate curves.

III. EXPERIMENTAL SETUP

The experimental campaign is conducted in the anechoic chamber at the University of Sherbrooke, using the setup depicted in Fig. 3. This measured configuration consists of a seven-bladed rotor, shroud and heat exchanger. To capture the far-field acoustic pressure radiated by the cooling module, an arc-shaped array with a radius of 1.8 meters is employed, consisting of thirteen microphones spaced at 15-degree intervals, covering a total of 180 degrees. Microphone 1 is positioned axially upstream, while microphone 13 is located axially downstream, perpendicular to the plane of rotation. The centre of the arc is aligned with the centre of the fan hub. The complete cooling module is mounted on a fixed frame rather than an ISO-5801 standard test plenum, meaning only the design condition is evaluated. Sound pressure data is collected using pre-polarized Brüel & Kjær (B&K) 1/4-inch condenser microphones, and the signals are simultaneously processed using a B&K front-end spectrum analyzer. The acoustic signals are sampled at a frequency of 65.536 kHz, with a frequency resolution of 3.125 Hz. Given the anechoic chamber's cut-off frequency of 80 Hz, only spectral data above this threshold is analyzed. More details can be found in [12].

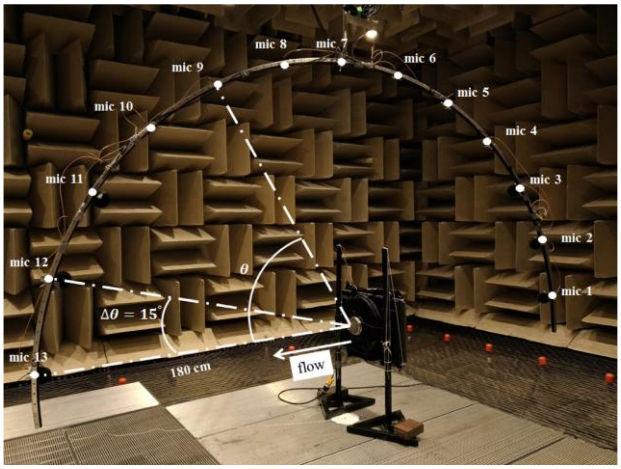

Figure 3: Experimental setup [12].

IV. NUMERICAL SETUP

The numerical simulations are performed using the hybrid LBM/Very Large Eddy Simulations implemented in the commercial software PowerFlow 6-2024-R4 version. Unresolved turbulence is modelled using a modified RNG k-ε approach with an incorporated swirl model [13]. The wall boundary layers are represented using a wall function that accounts for pressure gradient effects, as achieving small $y+$ values with a cartesian mesh is computationally expensive. Consequently, the velocity of voxels nearest to the wall is assumed to follow the wall-law profile. The whole domain is divided into ten variable resolution regions (VR) with three damping zones (DZ) i.e. like the wedges in the anechoic chamber. To reproduce the experimental setup, these zones, employ increasingly high isotropic viscosity (starting from the physical viscosity of VR4) to effectively absorb the reflected

waves and ensure the free field condition. The smallest donut VR covers the fan tip and blade area where the highest velocity gradients are expected. The heat exchanger and shroud are placed in the VR9 region. The resolution of remaining VR regions decreases by a factor of 2. The ceiling, floor and all walls are modelled as solid with no-slip and inlet, outlet with uniform pressure (static pressure with free flow direction) and reflection damping boundary conditions as shown in Fig.4. The HE of dimensions 549 mm × 389 mm × 17.8 mm is added 25 mm upstream of the fan hub and is modelled as an equivalent porous media, a technique previously validated against experimental data by Tebib [11]. The same porous media is used for this simulation. In equivalent porous media pressure loss depends on the inflow velocity, resulting in higher pressure loss for higher-velocity regions as demonstrated by Wang [14], see the resistance curve implemented for this simulation in Fig.5.

The simulation runs for a physical time of 0.53 seconds, covering a total of thirty fan revolutions. This setup results in a sampling frequency of 37.155 kHz, with a data recording period of ten timesteps. The physical timestep is set to 8.411×10^{-7} seconds, corresponding to approximately 4,000 timesteps per blade passage and around 28,000 timesteps per full revolution for seven-bladed configuration.

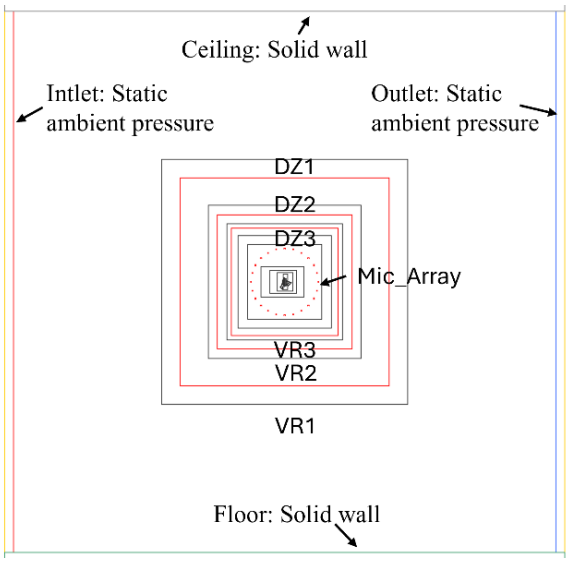

Figure 4: Simulation setup.

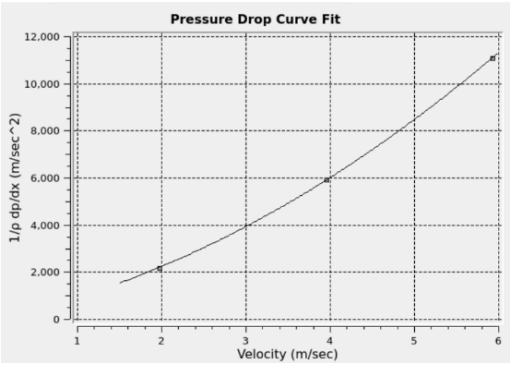

Figure 5: Resistance curve for heat exchanger.

To capture the radiated sound pressure, twenty-four direct microphone probes of diameter 6.35 mm, spaced every 15-degree are positioned around the module in the VR5 region, where the voxel (cubic element) size is 16 mm and the maximum achievable frequency is 9.66 kHz, using the five points per wavelength.

V. Results

This section describes the main findings of this study and their validation against the experimental data. The averaged flow behavior is first analyzed to understand the effects of solidity on the mean flow field. Finally, the sound spectrum and directivity are analyzed and correlated with the aerodynamic fluctuations.

A. Mean Velocity

The time-averaged flow field is analyzed in the meridional plane crossing the hub center to examine the flow behavior for each configuration. As shown in Fig. 6, rotor solidity does not significantly affect the mean flow field, with similar flow behavior observed under the same operating conditions. However, tip leakage flow increases in the thirteen-bladed configuration (black dashed ellipses). Both configurations exhibit uniform flow upstream of the fan, with smoother flow for cases including the HE. Downstream, the flow accelerates due to the work done by the fan. In the seven-bladed configuration, the entire blade contributes to flow acceleration. Conversely, in the thirteen-bladed fan, where the chord length is modified near the hub, less work is done by the hub region, and most of the acceleration occurs in the higher-radius blade span (black dashed squares). At the design point, the gap between the shroud and HE causes strong flow impingement, resulting in significant radial and tangential flow components in the tip region. For the thirteen-bladed configuration, the increased stagger angle creates a larger axial gap near the ring region compared to the seven-bladed fan, leading to higher velocity components impinging in this area.

B. Mean Pressure

The time-averaged static pressure distribution on the suction side of the fan surface is shown in Fig. 7. A consistent feature across all contours is the presence of a recirculation bubble beneath the ring, caused by leakage flow impingement. This bubble intensifies with increased rotor solidity. Additionally, transitioning from a seven-bladed to a thirteen-bladed configuration reduces the leading-edge vortex yielding the local low suction. This reduction can be attributed to the lower load per blade in the thirteen-bladed configuration, as the seven-bladed rotor operates at the same flow rate, resulting in a higher load on each blade to achieve equivalent work. The seven-bladed configuration exhibits higher static pressure near the hub up to mid-span, though this effect is less pronounced in the HE case, where slightly different incidence angle results in different stagnation points. In contrast, the thirteen-bladed configuration shows higher static pressure consistently along the leading edge, reducing flow velocity to nearly zero in this region.

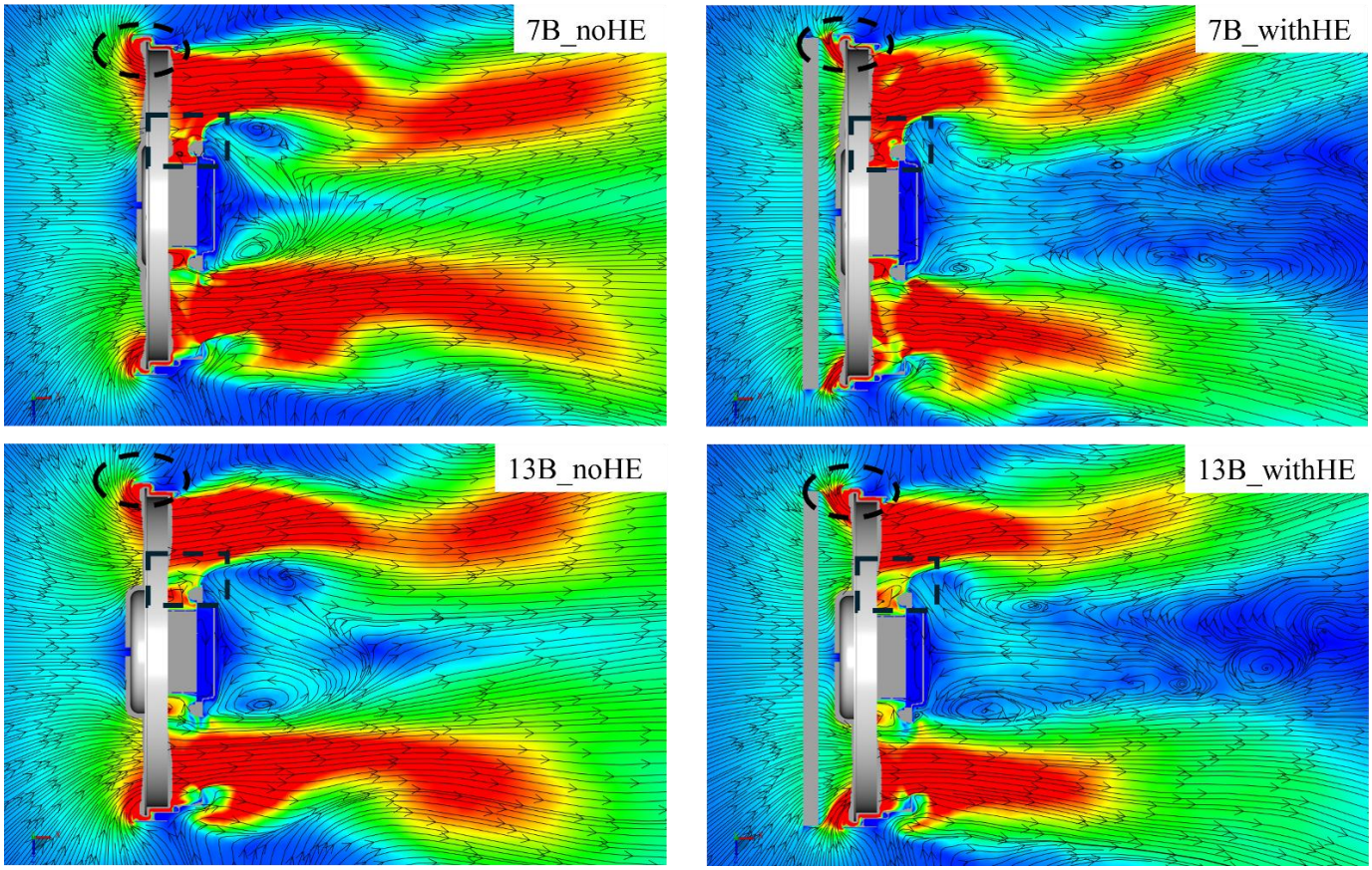

Figure 6: Time-averaged velocity field in a meridional cut.

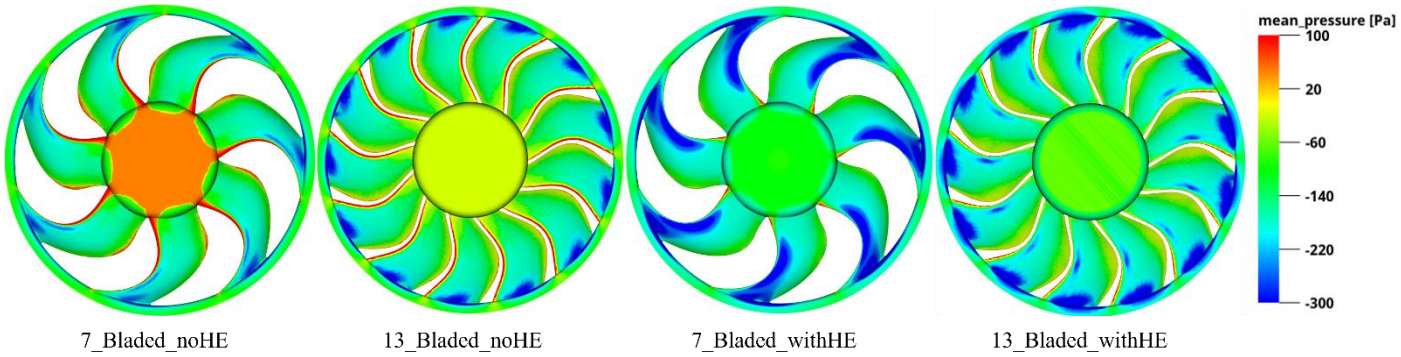

Figure 7: Time-averaged static pressure on the blade suction side.

C. Pressure Fluctuations

After analyzing the mean velocity and pressure distributions, the root mean square (RMS) of fluctuating pressure is extracted from the fan surface to identify noise sources, as pressure fluctuations are the primary contributors to noise according to acoustic analogy. Figure 8 shows that the most significant fluctuations occur near the tip region, where leakage flow impinges on the blade and a recirculation bubble forms. These fluctuations cover a larger tip region for both operating points in a thirteen-bladed configuration showing minimal fluctuations in the remaining blade surface. Apart from that higher solidity is mitigating the near hub fluctuations which are quite prominent for seven-bladed fans.

D. Rotor Forces

The axial loading integrated over the entire rotor is plotted in Figs. 9 (a) & (b) to analyze the thrust generated by each blade. Since the force per unit area is proportional to the loading, higher fluctuation levels in this force may lead to increased noise levels. Comparisons under identical conditions reveal

that the thirteen-bladed configuration exhibits higher fluctuations. Lateral forces are not included, as both rotors maintain good radial equilibrium, resulting in negligible levels of these forces.

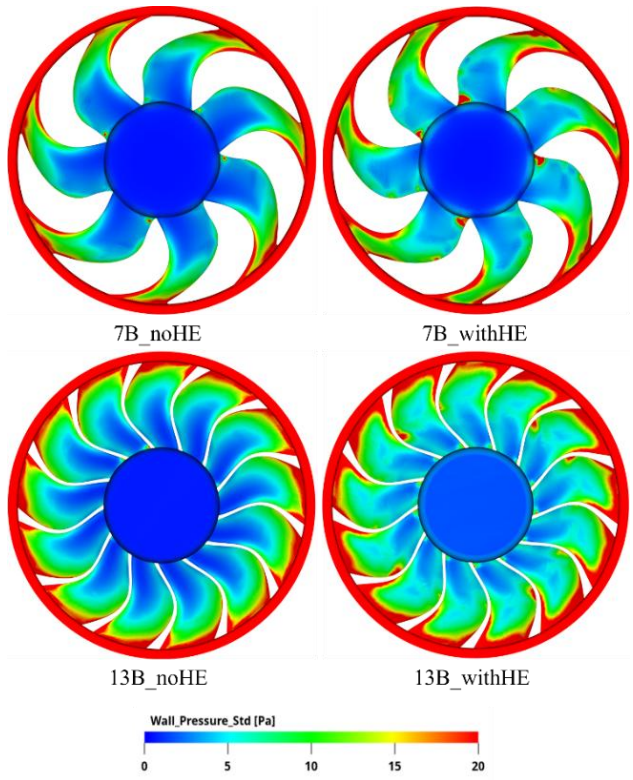

Figure 8: RMS of the fan surface pressure fluctuations on the suction side.

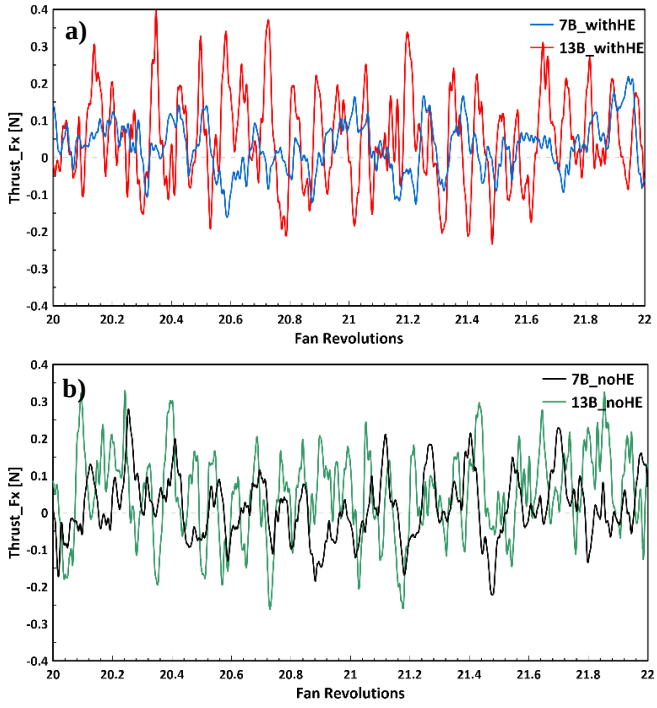

Figure 9: Integral of axial forces for a) withHE, and b) noHE configurations.

E. Acoustic Field

The far-field pressure spectrum, obtained via direct probes as detailed in the numerical setup, is compared in Fig. 10 (a) for HE configurations against experimental data acquired using the microphone placed on the rotational axis (upstream). Good agreement is found at mid-frequencies (f/BPF~5-10). At low frequencies, the LBM result overpredicts the noise levels most likely because of the fan deflection that closes the tip gap and significantly reduces the noise levels below f/BPF~5 as already shown on the seven-bladed configuration by Tebib [11]. The effect of increased solidity is clearly observed in this frequency range, with higher amplitude and pronounced sub-harmonic humps appearing before the blade passing frequency (BPF) and its harmonics. This phenomenon is likely attributed to leakage flow, which predominantly influences this portion of the spectrum as shown by Sanjose [10]. The discrepancy observed at higher frequencies between numerical spectrums is due to the scaling effect applied to match the blade passing tones, while the differences in the experimental spectrum result from system response that could be alleviated by removing acoustic diffraction effects as shown by Pasco [15]. Apart from that, the 7-blade spectrum accurately captured the pattern for the 1st BPF, exhibiting the correct width and peak emergence value in alignment with the test results. Furthermore, a comparison of the four configurations in Fig. 10 (b) highlights the effect of solidity on radiated noise. The increased solidity influences the lower frequency range by leaving the higher frequency spectrum unaltered. The higher amplitude of the thirteen-bladed rotor narrowband is likely due to higher thrust fluctuations seen previously. However, configurations of the same rotor produce similar spectra, except for a slightly higher tonal peak in the case without the HE, which could be attributed to increased axial thrust.

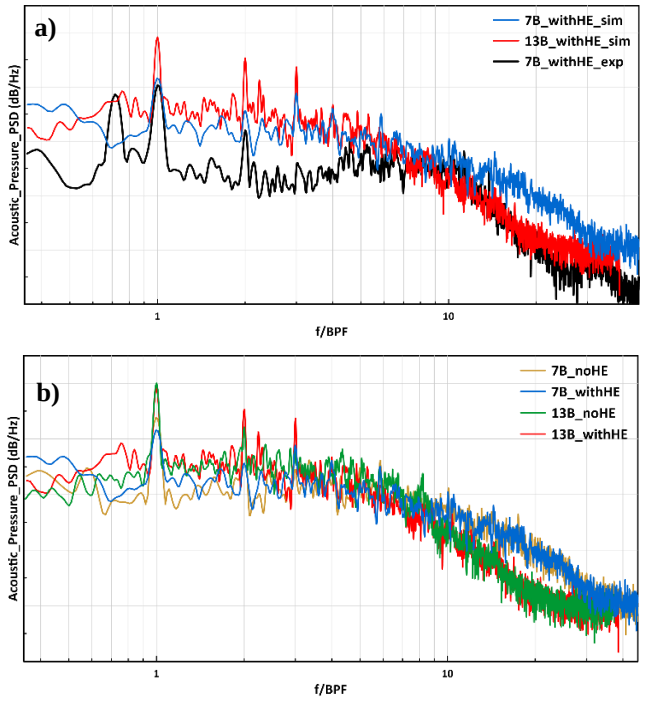

Figure 10: Spectrum comparison of a) withHE configurations, and b) all numerical configurations.

The directivity pattern for both operating points is analyzed against experimental data obtained using the microphones shown in Fig. 2 for the design point. Overall, the numerical results have a similar shape to the experimental data, as all curves exhibit a dipole along the rotational axis. However, the amplitude is overpredicted, which can be attributed to the differences observed in the spectra below ~1kHz. The thirteen-bladed configuration experiences higher tip leakage flow and axial thrust, leading to increased amplitudes of radiated noise in all directions. Comparing the two configurations shows that the directivity pattern remains largely unchanged across operating points, but higher amplitudes are observed with the increased number of blades.

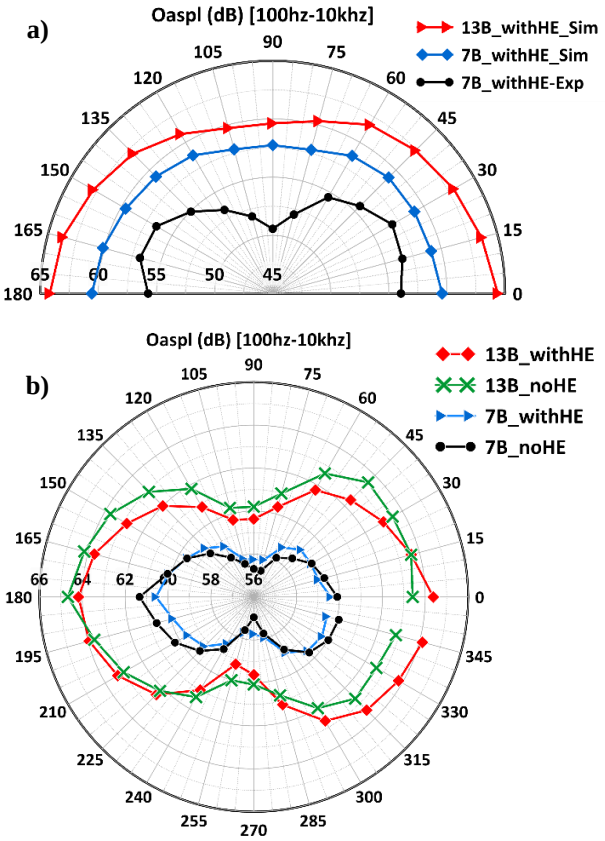

Figure 11: Directivity comparison of a) withHE, and b) all numerical configurations.

VI. Conclusion

The effect of rotor solidity on an automotive cooling unit is analyzed under free discharge and design point conditions, ensuring consistent flow rate and axial stacking parameters. A special rotor with increased solidity is designed, featuring a larger chord length above the mid-span—where most loading occurs—and a reduced chord length near the hub, combined with a blade count of thirteen. The results indicate that for the considered configurations, increased solidity leads to higher noise levels, contrary to expectations that reduced rotational speed would lower noise levels, as radiated sound power is often said to scale with the sixth power of speed. This increase in noise is attributed to intensified leakage flow caused by pressure differences across the rotor and greater axial force fluctuations, even at the same mass flow rate. However, the operating point has minimal impact on both amplitude and directivity, with only a slight increase in narrowband peak amplitude under free discharge conditions. Numerical results are compared with experimental data obtained from the anechoic chamber at the University of Sherbrooke, showing reasonable agreement in sound pressure level spectra and directivity above 1.5 kHz. Discrepancies at lower frequencies are likely due to rotor deformation in experiments, which reduces the tip gap.

VII. References

[1] M. Henner, B. Demory, M. Alaoui, M. Laurent, and B. Behey, "Effect of blade curvature on fan integration in engine cooling module," *Acoustics*, vol. 2, no. 4, pp. 776-790, 2020.

[2] K. Bamberger, T. Carolus, and M. Haas, "Optimization of low-pressure axial fans and effect of subsequent geometrical modifications," *Proc. Fan*, 2015.

[3] F. Krömer, J. Müller, and S. Becker, "Investigation of aeroacoustic properties of low-pressure axial fans with different blade stacking," *AIAA Journal*, vol. 56, no. 4, pp. 1507-1518, 2018.

[4] M. Masi, P. Danieli, and A. Lazzaretto, "Effect of solidity and aspect ratio on the aerodynamic performance of axial-flow fans with 0.2 hub-to-tip ratio," *Journal of Turbomachinery*, vol. 145, no. 8, 2023.

[5] C. Sarraf, H. Nouri, F. Ravelet, and F. Bakir, "Experimental study of blade thickness effects on the overall and local performances of a controlled vortex designed axial-flow fan," *Experimental Thermal and Fluid Science*, vol. 35, no. 4, pp. 684-693, 2011.

[6] E. Tannoury, B. Demory, M. Henner, P.-A. Bonnet, P. Caule, and Y. Creteur, "A design of experiment for evaluating installation effects and the influence of blade loading on the aeroacoustics of an automotive engine cooling fan. ," in *Proceedings of FAN 2012*.

[7] T. Fukano, Y. Kodama, and Y. Takamatsu, "Noise generated by low-pressure axial flow fans, II: Effects of number of blades, chord length and camber of blade," *Journal of Sound and Vibration*, vol. 50, no. 1, pp. 75-88, 1977.

[8] E. Antoniou, G. Romani, A. Jantzen, F. Czwielong, and S. Schoder, "Numerical flow noise simulation of an axial fan with a Lattice-Boltzmann solver," *Acta Acustica*, vol. 7, p. 65, 2023.

[9] D. Lallier-Daniels, M. Piellard, B. Coutty, and S. Moreau, "Aeroacoustic study of an axial engine cooling module using Lattice-Boltzmann simulations and the Ffowcs Williams and Hawkings' analogy," *European Journal of Mechanics-B/Fluids*, vol. 61, pp. 244-254, 2017.

[10] S. Moreau and M. Sanjose, "Sub-harmonic broadband humps and tip noise in low-speed ring fans," *The Journal of the Acoustical Society of America*, vol. 139, no. 1, pp. 118-127, 2016.

[11] S. Tebib *et al.*, "Detailed noise analysis of automotive engine cooling modules using the Lattice-Boltzmann Method," in *AIAA AVIATION 2023 Forum*, 2023, p. 3205.

[12] O. Amoiridis *et al.*, "Sound localization and quantification analysis of an automotive engine cooling module," *Journal of Sound and Vibration*, vol. 517, p. 116534, 2022.

[13] H. Chen, S. A. Orszag, I. Staroselsky, and S. Succi, "Expanded analogy between Boltzmann kinetic theory of fluids and turbulence," *Journal of Fluid Mechanics*, vol. 519, pp. 301-314, 2004.

[14] Z. Wang *et al.*, "Numerical and experimental investigation on the integrate performance of axial flow cooling fan and heat exchanger," *Applied Thermal Engineering*, vol. 245, p. 122814, 2024.

[15] Y. Pasco and S. Moreau, "Sound radiation of a smoke-removal fan system," *Acta Acustica united with Acustica*, vol. 105, no. 1, pp. 86-94, 2019.